Remote sensing of terrestrial snow water equivalent using satellite-based radiometer sensors

Pinja Venäläinen

Aalto University

Aalto University publication series
Doctoral Theses 90/2025

Remote sensing of terrestrial snow water equivalent using satellite-based radiometer sensors

Pinja Venäläinen

A doctoral thesis completed for the degree of Doctor of Science (Technology) to be defended, with the permission of the Aalto University School of Electrical Engineering, at a public examination held at the lecture hall M1 of the school on 19 May 2025 at 12:00.

Aalto University
School of Electrical Engineering
Department of Electronics and Nanoengineering

Supervising professor
Associate Professor Jaan Praks, Aalto University, Finland

Thesis advisors
Dr. Kari Luojus, Finnish Meteorological Institute, Finland

Preliminary examiners
Dr. Edward Kim, NASA, USA
Dr. Julien Meloche, Environment and Climate Change Canada, Canada

Opponent
Associate Professor Nick Rutter, Northumbria University, United Kingdom

Aalto University publication series
Doctoral Theses 90/2025

Image on the cover: Mirkka Hämäläinen

ISBN 978-952-64-2542-9 (soft cover)
ISBN 978-952-64-2541-2 (PDF)
ISSN 1799-4934 (printed)
ISSN 1799-4942 (PDF)

http://urn.fi/URN: ISBN:978-952-64-2541-2

Unigrafia Oy
Helsinki 2025

Aalto University

ABSTRACT

Author Pinja Venäläinen

Name of the doctoral thesis Remote sensing of terrestrial snow water equivalent using satellite-based radiometer sensors

Article-based thesis

Number of pages 116

Keywords remote sensing, snow cover, passive microwave radiometers

Seasonal snow cover is an important component of the Earth's hydrological and energy cycles, affecting water resources and climate feedback mechanisms. Snow water equivalent (SWE), representing the water content of a snowpack, is a key characteristic of snow cover. SWE estimates can be retrieved from passive microwave radiometer data. Global satellite-based passive microwave radiometer measurements are available from 1978 onwards allowing construction of long SWE time series. Radiometer-based SWE retrievals can be improved with the assimilation of synoptic snow depth observations. This thesis aims to advance assimilation-based SWE retrieval method with parametrization of snow density and bias correction.

Publication I presents a method for creating climatological spatially and temporally dynamic snow density fields. The effect of post-processing SWE retrieval with these fields is also studied in the publication. Post-processing improves the overestimation of small SWE values and small improvements in the underestimation of large SWE values are also present.

Publication II investigates implementing dynamic snow densities into the SWE retrieval. Similarly to post-processing with dynamic snow densities, implementing them into the retrieval improves the accuracy of (small) SWE estimates. Additionally, the reduction in hemispheric peak snow mass seen when post-processing with dynamic snow densities is smaller when snow densities are implemented into the SWE retrieval. Implementation of dynamic snow densities into SWE retrieval also delays peak snow mass timing and thus improves the seasonal evolution of SWE.

Publication III updates previously studied monthly bias correction method for monthly SWE estimates with new reference data. Monthly bias correction is also expanded to a daily time scale in this publication. Updated monthly bias correction improves monthly estimates and daily bias correction slightly improves the accuracy of large SWE estimates. More importantly adds a significant amount of snow to the hemispheric snow mass estimation.

Together these three studies improve SWE estimations and our ability to monitor seasonal snow cover.

Aalto-yliopisto

TIIVISTELMÄ

Tekijä Pinja Venäläinen

Väitöskirjan nimi Maanpäällisen lumen vesiarvon kaukokartoitus Satelliittimikroaaltoradiometreillä

Artikkeliväitöskirja

Sivumäärä 116

Avainsanat kaukokartoitus, lumi, passiivimikroaaltoradiometri

Kausittainen lumipeite on tärkeä osa maapallon vedenkiertokulkua ja säteilytasapainoa. Lumen vesiarvo, joka kuvaa lumipeitteen vesipitoisuutta, on keskeinen lumipeitettä kuvaava määre. Lumen vesiarvoa voidaan arvioida passiivimikroaaltokaukokartoituksella. Satelliittimikroaaltoradiometri mittauksia on saatavilla vuodesta 1978 alkaen, mikä mahdollistaa pitkien lumen vesiarvo aikasarjojen laatimisen. Radiometrimittauksiin perustuvia vesiarvo arviota voidaan parantaa hyödyntämällä lumen syvyysmittauksia vesiarvon arvioinnissa. Tämä väitöskirja pyrkii kehittämään lumensyvyys mittauksia hyödyntävää lumen vesiarvon kaukokartoitusmenetelmää parametrisoimalla lumentiheyden sekä harhakorjauksella.

Julkaisu I esittelee menetelmän ajan ja paikan suhteen dynaamisten lumentiheyskenttien luomiseen. Julkaisussa tutkitaan myös näiden lumentiheyskenttien vaikutusta satelliittimikroaalto pohjoisiin lumen vesiarvo arvioihin jälkikäsittelyn avulla. Jälkikäsittely parantaa pienten arvojen yliarviointia sekä tuottaa pieniä parannuksia suurten vesiarvojen aliarviointiin.

Julkaisussa II tutkitaan dynaamisten lumitiheyksien integroimista lumen vesiarvo arviointimenetelmään. Samoin kuin dynaamisilla lumitiheyksillä jälkikäsitellessä myös niiden sisällyttäminen arviointimenetelmään parantaa pienten arvioiden tarkkuutta. Lisäksi pohjoisen pallonpuoliskon lumimassan huippuarvon pieneneminen, joka havaittiin dynaamisilla lumitiheyksillä jälkikäsitellessä, pienenee kun lumentiheydet integroidaan arviointimenetelmään. Dynaamisten lumitiheyksien sisällyttäminen vesi arvo arviointiin myös viivästyttää lumimassan huipun ajoitusta ja parantaa siten arviota kausittaisen lumen kehityksestä.

Julkaisussa III päivitetään kuukausittaisten vesi arvojen harhan korjausmenetelmä uusilla vertailutiedoilla. Harhan korjausmenetelmää laajennetaan myös päivittäiselle aikaskaalalle. Päivitetty kuukausittainen harhakorjaus parantaa kuukausittaisia kaukokartoitus arvioita lumen vesi arvosta. Päivittäinen harhakorjaus parantaa hieman suurten vesiarvojen tarkkuutta ja ennen kaikkea lisää merkittävästi lunta pohjoisen pallonpuoliskon lumimassa-arvioihin.

Yhdessä nämä kolme tutkimusta parantavat satelliittimikroaaltoradiometri mittauksiin pohjautuvia lumen vesiarvo arvioita ja kykyämme tarkkailla kausittaista lumipeitettä.

Preface

The research presented in this thesis was carried out at the Finnish Meteorological Institute between 2020-2025. Work was conducted as part of the ESA SnowCCI+ project. I have received help and support from many people during this time, and I would like to express my sincere thanks to all of them.

I would like to express my gratitude to my advisor, Dr. Kari Luojus, for his invaluable guidance, support, and encouragement over the course of this research. My sincere thanks go to my supervisor, Prof. Jaan Praks, for his long-standing support throughout my academic journey, from advising my bachelor's thesis and supervising my master's thesis to guiding me through the dissertation process.

I am thankful to the pre-examiners, Dr. Ed Kim and Dr. Julien Meloche, for their valuable comments and suggestions during the pre-examination. I also wish to thank Prof. Nick Rutter for kindly agreeing to act as the opponent at my thesis defense.

I would also like to express my sincere thanks to Prof. Jouni Pulliainen, Dr. Juha Lemmetyinen, and Dr. Matias Takala. Their long-standing work on this topic laid the foundation for much of this thesis, and I have greatly benefited from their expertise and the opportunity to collaborate with them. I extend my appreciation to my colleagues in the Satellite Services and Research group for their collaboration, support, and for providing a positive working environment. I would also like to thank Dr. Colleen Mortimer and Dr. Lawrence Mudryk from Environment and Climate Change Canada. Their feedback during the article writing process was highly appreciated.

I am thankful to my friends for the laughter and good moments that helped bring balance to this process. I am especially grateful to my family for their steady support throughout. To my parents, Leena and Ari, thank you for your constant encouragement. Finally, I want to thank my partner, Alex. I could not have wished for a better companion for this journey.

Espoo, April 15, 2025,

Pinja Venäläinen

Contents

Abbreviations

AMSR2 Advanced Microwave Scanning Radiometer - 2

AMSR-E Advanced Microwave Scanning Radiometer for EOS

CDR Climate Data Record

DMSP Defense Meteorological Satellite Program

EASE Equal-Area Scalable Earth

ECMWF European Centre for Medium-Range Weather Forecasts

FMI Finnish Meteorological Institute

FY-3 Fengyung-3

GHCNd Global Historical Climatology Network daily

GSv3.0 GlobSnow v3.0 dataset

HUT Helsinki University of Technology

IDW Inverse Distance Weighted

IDWR Inverse Distance Weighted Regression

MWRI Microwave Radiation Imager

NASA National Aeronautics and Space Administration

NOAA National Oceanic and Atmospheric Administration

PMW Passive microwave

RIHMI-WDC All-Russia Research Institute of Hydrometeorological Information - World Data Center

RMSE Root-mean-squared error

SCv3.1 SnowCCI v3.1 dataset

SD Snow Depth

SMMR Scanning Multichannel Microwave Radiometer

SSM/I Special Sensor Microwave/Imager

SSMIS Special Sensor Microwave Imager/Sounder

SWE Snow water equivalent

Symbols

B Spectral radiance

$BIAS$ Bias

c Velocity of light in vacuum

d_o Effective snow grain size

d_{obs} Snow grain size

e Emissivity

$EST_{i,t}$ Radiometer estimate of SWE at location i at time t

f Frequency

h Planck's constant

k_B Boltzmann's constant

$REF_{i,t}$ Reference SWE observation at location i at time t

SD Snow depth

SWE Snow water equivalent

T Physical temperature

T_b Brightness temperature

$T_{b,mod}$ Modelled brightness temperature

$T_{b,obs}$ Measured brightness temperature

T_s Physical temperature of snow

$w_{1,i}$ Weight of first month on i_{th} day

$w_{2,i}$ Weight of first month on i_{th} day

κ_a Absorption coefficient

κ_e Extinction coefficient

κ_s Scattering coefficient

λ Wavelength

$\rho_{constant}$ Constant density of snow

$\rho_{dynamic}$ Dynamic density of snow

σ Standard deviation

σ^2 Variance

List of Publications

This thesis consists of an overview and of the following publications which are referred to in the text by their Roman numerals.

I Pinja Venäläinen, Kari Luojus, Juha Lemmetyinen, Jouni Pulliainen, Mikko Moisander, and Matias Takala. Impact of dynamic snow density on GlobSnow snow water equivalent retrieval accuracy. *The Cryosphere*, 15, 2969–2981, https://doi.org/10.5194/tc-15-2969-2021, June 2021.

II Pinja Venäläinen, Kari Luojus, Colleen Mortimer, Juha Lemmetyinen, Jouni Pulliainen, Matias Takala, Mikko Moisander, and Lina Zschenderlein. Implementing spatially and temporally varying snow densities into the GlobSnow snow water equivalent retrieval. *The Cryosphere*, 17, 719-736,https://doi.org/10.5194/tc-17-719-2023, February 2023.

III Pinja Venäläinen, Colleen Mortimer, Kari Luojus, Lawrence Mudryk, Matias Takala, and Jouni Pulliainen. Updated monthly and new daily bias correction for assimilation-based passive microwave SWE retrieval. Submitted to *The Cryosphere*, November 2024.

Author's Contribution

Publication I: "Impact of dynamic snow density on GlobSnow snow water equivalent retrieval accuracy"

The author designed the study with KL, JL, and JP. The author was responsible for collecting, processing and analysing the data. The author was responsible for writing the manuscript which was reviewed, edited, and approved by all coauthors.

Publication II: "Implementing spatially and temporally varying snow densities into the GlobSnow snow water equivalent retrieval"

The author, KL, JL, and JP designed the study. The author was the main developer for updating the algorithm and was responsible for generating different datasets and analysing them. The author also produced the first draft of the manuscript which was edited together with coauthors.

Publication III: "Updated monthly and new daily bias correction for assimilation-based passive microwave SWE retrieval"

The study was designed by the author, KL and JP. The author was the main contributor to method development. The author was also responsible for generating the new data records. The author performed data analyses with coauthors. The author also produced the first draft of the manuscript which was edited together with coauthors.

1. Introduction

Understanding seasonal snow cover, and its spatial and temporal variations and changes, is essential. Each year, seasonal snow covers nearly half of the Northern Hemisphere's land mass (R. D. Brown and Robinson, 2011) (example seen in Figure 1.1) and plays a crucial role in hydrological and energy cycles (Barnett et al., 2005; Flanner et al., 2011). Snow cover stores winter precipitation, releasing it as runoff when temperatures rise in spring and summer. This meltwater is a significant source for many rivers and reservoirs, and around one-sixth of the world's population relies on snow as their primary source of drinking water (Barnett et al., 2005). Additionally, water released from the snowpack is an important source of hydropower (Magnusson et al., 2020) and it can also cause flooding (Bell et al., 2016).

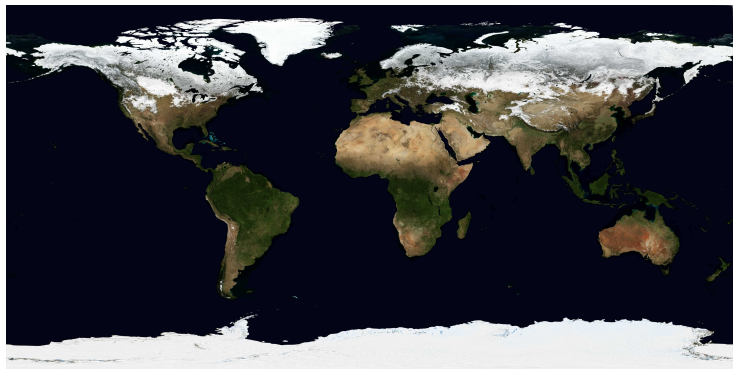

Figure 1.1. Seasonal snow covers a significant portion of the Northern Hemisphere's land mass yearly. Example of snow cover extent in March 2004 observed by the MODIS spectrometer onboard the Terra satellite (Stöckli et al., 2005).

Snow cover has a higher albedo than bare ground, reflecting a substantial portion of incident solar radiation back into space and cooling temperatures (R. L. Armstrong and Brun, 2008). A shorter snow season over a smaller spatial domain can lead to a positive feedback loop, potentially playing a major role in global warming (Qu and Hall, 2007; Flanner et al., 2011). For all these reasons, terrestrial snow is one of the Essential Climate Variables determined by the World Meteorological Organization (Bojinski et al., 2014).

Information about the current state and long-term climate data records (CDR) of snow cover are vital.

Snow water equivalent (SWE) is an important parameter for describing the state of the snow pack. SWE is the amount of water that would be released if all the snow in a snow pack melted at once. In situ ground measurements from weather stations or snow surveys are often used for estimating SWE (Kinar and Pomeroy, 2015). However, in situ measurements are often spatially, and in many cases also temporally, sparse, which limits their usefulness on a global scale (Broxton et al., 2016). Remote sensing offers a good alternative for ground-based measurements as it can provide daily observations on a global scale.

Passive microwave (PMW) remote sensing is particularly suitable for monitoring snow cover. Unlike optical instruments, PMW does not rely on sunlight, enabling high-latitude observations even during polar night (Ulaby et al., 2014). PMW observations are also relatively insensitive to clouds and rain and can detect characteristics of the entire snowpack, whereas optical sensors generally capture only surface information. Additionally, global PMW observations have been available daily since 1987 (and every other day since 1978), supporting the creation of long-term CDRs.

The first global PMW-based SWE retrieval algorithm was introduced in 1987 (A. Chang and Foster, 1987). This and other early retrieval algorithms were purely empirical and based on a linear regression between snow depth and the difference between PMW measurements made at two different frequencies (often 19 GHz and 37 GHz) (e.g. Kunzi et al., 1982; Goodison, 1989). Over the years, the development of global PMW SWE retrievals has continued (e.g. J. Foster et al., 1997; Pulliainen, 2006; Kelly, 2009; Tedesco and Jeyaratnam, 2016; J. Yang et al., 2024).

However, SWE retrievals based solely on PMW data often have high uncertainties and fail to meet user accuracy requirements (e.g. Mudryk et al., 2015; Mortimer et al., 2020). One option to improve SWE retrieval is to combine PMW data with in situ ground snow depth measurements. An approach that utilizes Bayesian iterative assimilation to combine PMW data with a semi-empirical radiative transfer model together with a priori snow depth estimation from in-situ measurements has been studied by Pulliainen, 2006 and Takala et al., 2011 and has been shown to produce SWE estimates with improved accuracy (Mortimer et al., 2020). This thesis studies possibilities to improve assimilation-based PMW SWE retrieval and thus improve our ability to monitor seasonal snow cover. The two main targets of improvement studied in this thesis are: a) the parametrization of snow density, and b) the limited ability to retrieve large SWE values.

The assimilation-based SWE retrieval method assumes a constant snow density, independent of snow depth, location, and season (Takala et al., 2011). This simplification introduces uncertainty, as snow density varies with environmental conditions and changes over time and location. Publi-

cations I and II present alternative approaches for creating spatially and temporally dynamic climatological snow density fields based on historical snow density measurements. In Publication I, these dynamic snow densities are used for post-processing assimilation-based SWE retrieval products, and in Publication II, these densities are implemented into the actual SWE retrieval.

PMW SWE retrievals have limited ability to retrieve large SWE values as snowpack changes from a scattering medium to a source of emission at large SWE values (SWE $>$ 150 mm). While the data assimilation improves the estimation of moderate snowpacks (SWE $<$ 200 mm), retrieval of large SWE values remains challenging. One approach to improve the estimation of large SWE values is bias correction, which was first introduced in 2020 by Pulliainen et al., 2020. In this paper, bias corrected assimilation-based SWE product was used to form an accurate estimation of March snow mass between 1979-2018. This bias correction method is updated in Publication III using new reference data and expanded from a monthly to a daily time scale.

This thesis is divided into the following chapters: Chapter 2 describes the concept of remote sensing with a focus on microwave radiometry. Radiometer-based SWE retrievals are also discussed in Chapter 2. Chapter 3 presents the main findings of Publications I and II, explaining how temporally and spatially varying snow densities can improve SWE retrieval. Chapter 4 focuses on bias correction and presents the main results of Publication III. Chapter 5 presents a discussion, and finally, Chapter 6 concludes the work.

2. Passive microwave remote sensing of SWE

This chapter introduces the general concept of remote sensing and explains the theory and principles of microwave radiometry. It also gives a brief overview of different passive microwave SWE retrievals and a more detailed overview of the assimilation-based SWE retrieval.

2.1 Remote sensing

Remote sensing is the science of gathering information about a target without direct physical contact. This information is collected by measuring reflected or emitted electromagnetic radiation from the target, often from a spacecraft. Most of the electromagnetic spectrum can be used for remote sensing; however, the microwave and visible light spectrums are most commonly utilised for remote sensing of snow. These spectrums fall within atmospheric windows, where the atmosphere is mostly transparent to these frequencies; frequencies outside these windows are mostly absorbed by the atmosphere (Weng, 2011).

Remote sensing sensors can be passive or active. Active instruments send out a pulse of energy that is reflected from a target and observe changes in the reflected signal. Active sensors provide their own source of energy to illuminate the target. This differs from the passive instruments, which do not illuminate the target with their own signal but observe radiation naturally emitted or reflected by the environment. Passive optical spectrometers are often used for measuring snow cover extent (e.g. Metsämäki et al., 2012; Dozier et al., 2009), while active optical lidars can measure surface heights and, thus, snow depths (Deems et al., 2013). However, optical remote sensing is limited by cloud cover and depends on solar radiation for illumination, which is problematic at high latitudes during mid-winter (Metsämäki et al., 2015; Frei et al., 2012).

Both active (radars) and passive (radiometers) microwave sensors can be used to study snow. Some active microwave instruments (synthetic aperture radars) can offer higher resolution than passive microwave radiometers

but often have more limited spatial and temporal coverage. Studies have explored using radars for estimating SWE, particularly in mountainous areas where higher spatial resolution is needed for acquiring accurate information (Lievens et al., 2019). However, as global daily passive microwave measurements have been available since June 1987 and global measurements from every second day since 1978, radiometer data can be used to construct long-term CDRs of snow characteristics.

2.1.1 Passive microwave remote sensing

All natural matter emits electromagnetic radiation due to the thermal movement of particles within the object. This radiation can be studied using the concept of a blackbody. A blackbody is an idealized object that both absorbs all incident radiation and emits all of its thermal energy; it is a perfect absorber and emitter. The energy radiated, or its spectral radiance B [$\mathrm{W\,sr^{-1}\,m^{-2}}$], by a blackbody is given by Plack's law (Planck, 1901):

$$B = \frac{2hf^3}{c^2}\left(\frac{1}{e^{hf/k_BT} - 1}\right), \tag{2.1}$$

where h is the Planck's constant ($6.634x10^{-34}$ J), f is the frequency (Hz), c is the speed of light ($2,998x10^8$ $\mathrm{ms^{-1}}$), k_B is the Boltzmann's constant (1.38×10^{-23} $\mathrm{JK^{-1}}$) and T is physical temperature of the radiator (in Kelvins). In the microwave range, when $hf << k_BT$, the Rayleigh-Jeans approximation can be used to estimate the B (Ulaby et al., 2014):

$$B = \frac{2k_BT}{\lambda^2}, \tag{2.2}$$

where wavelength $\lambda = \frac{c}{f}$. This equation implies that the energy emitted by a black body, B, is linearly dependent on physical temperature T.

However, natural targets are not black bodies; they are not perfect emitters or absorbers. Brightness temperature (T_b [K]) is the equivalent physical temperature of a blackbody that would emit the same amount of energy as the real target at physical temperature T at a given frequency. The relationship between T_b and real kinetic temperature is defined as emissivity e (Ulaby et al., 2014):

$$e = \frac{T_b}{T}. \tag{2.3}$$

The emissivity depends on used frequency, polarization, and incidence angle. It is also dependent on the electromagnetic properties of the material, such as permittivity and permeability.

If the physical temperature of a target is known or can be deduced, we can calculate the emissivity of the target by measuring the T_b of the target with

a radiometer. Physical properties of the target, such as SWE in the case of snowpack, determine electromagnetic properties (including emissivity) of the target. Models (theoretical, empirical or semi-empirical) can be used to relate radiometer T_b measurements to physical properties.

In a typical passive microwave remote sensing scenario, the brightness temperature measured by a radiometer is composed of radiation from several sources. Figure 2.1 illustrates a scenario of a radiometer measuring the snow-covered ground. Radiometers measure radiation originating from a) solar and cosmic radiation, b) atmosphere, c) vegetation, d) snow, and e) soil. The propagation of radiation in different natural (lossy) media can be described using radiative transfer theory. It accounts for the absorption, emission, and scattering of radiation as it travels through materials like the atmosphere and snow.

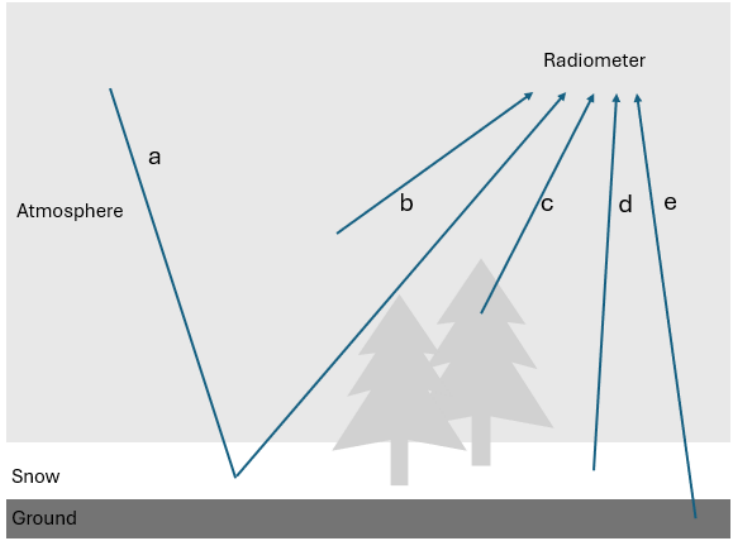

Figure 2.1. Radiation sources measured by spaceborne radiometer are a) solar and cosmic radiation, b) atmosphere, c) vegetation, d) snow and e) soil.

2.2 Radiometer remote sensing of SWE

The first global snow depth algorithm was introduced in 1987 by A. Chang and Foster, 1987. First snow retrieval algorithms were purely empirical and based on linear regression between snow depth and differences in observed T_b values measured using K-band (typically around 19 GHz) and Ka-band (typically around 36 GHz) (e.g. M. T. Hallikainen and Jolma, 1992; Goodison, 1989).

As a microwave signal propagates from the ground through dry snow, it undergoes absorption, scattering, or transmission through the snowpack, depending on the properties of the snowpack and the frequency of the

signal. When the wavelength of the signal is comparable to the snow grain size (approximately 36 GHz), scattering dominates, and the signal is attenuated. Attenuation increases with the accumulation of SWE until a limit of approximately 150 mm of SWE is reached. As the wavelength increases (approximately 19 GHz), transmission becomes dominant, and signal attenuation weakens. Frequencies below 10 GHz (wavelength larger than 3 cm) have no sensitivity to snow. Thus, the difference in measured T_b between 36 GHz and 19 GHz can be related to physical properties, specifically the amount, of snow.

Over the years, different enhancements have been proposed for the channel difference-based SWE retrievals. Foster et al. (1997) modified the SWE retrieval algorithm to take forest cover fraction into account. Kelly (2009) proposed dynamically adjusting coefficients that account for the evolution of snow grain size and the influence of vegetation and address deeper snowpacks. Building on dynamically adjusting coefficients, Tedesco and Jeyaratnam (2016) utilised artificial neural networks and snow emission modelling to determine coefficients. More recently, an operational SWE retrieval algorithm that utilises a traditional empirical equation but with fitting coefficients determined pixel-by-pixel based on high accuracy SWE reference dataset made using a random forest model coupled with an emission model was proposed by Yang et al. (2024).

There are, however, multiple sources of error in retrieving SWE values from radiometer data using empirical methods. When snow is shallow, differences in T_b measurements are minor, and estimating SWE is difficult (Tedesco, 2015). On the other hand, estimating large SWE values is also challenging. When the snowpack is deep (typically when SWE $>$ 150 mm), it transitions from a scattering medium to an emission source, and volume scattering is no longer dominant in the Tb response at 36 GHz (Takala et al., 2011; Derksen and Brown, 2012). Microwave measurements are also sensitive to the presence of liquid water and often do not perform well under wet snow conditions (Takala et al., 2011). Microwaves do not penetrate water (the presence of liquid water makes snow highly absorptive), and in wet snow conditions, only the top layer of snow above the uppermost wet portion of snow, if any, is detected.

Another approach for radiometer-based SWE retrieval is to use theoretical or semi-empirical models. In these cases, snow depth is estimated by fitting snow parameters in an electromagnetic model to minimize the difference between measured and modelled T_b (Tedesco, 2015). One problem with these methods is that different combinations of snow parameters can produce very similar T_b values. Thus, the solution for the model is not unique (Tedesco, 2015). The performance of passive microwave retrieval algorithms based on radiative transfer models can be improved with data assimilation (Pulliainen, 2006). This technique compares passive microwave data with a semi-empirical radiative transfer model assimilated

with ground-based snow depth measurements. The model also considers uncertainties of the radiative-transfer model, ground measurements, and the radiometer. This approach exploits the benefits of both satellite and in situ measurements. The semi-empirical assimilation approach used in this thesis is explained in more detail in Section 2.3.

2.2.1 Spaceborne radiometer systems for snow monitoring

Scanning Multichannel Microwave Radiometer (SMMR) was the first operational satellite-based radiometer instrument. It was developed and operated by the National Aeronautics and Space Administration (NASA), and its primary purpose was to study ocean surfaces with five different microwave frequencies (Gloersen and Barath, 1977). However, the frequencies measured are also suitable for monitoring snow. It was launched in October 1978 aboard the Nimbus-7 spacecraft. The Special Sensor Microwave/Imager (SSM/I), a seven-channel, four-frequency radiometer, was the successor of the SMMR instrument. The first SSM/I instrument was launched aboard Defense Meteorological Satellite Program (DMSP) satellite F8 in June 1987 (Hollinger et al., 1990). Since then, SSM/I instruments have been onboard five other DMSP satellites (F10-F15). Special Sensor Microwave Imager/-Sounder (SSMIS) was designed as the successor of the SSM/I instrument with 24 channels and 21 frequencies (Kunkee et al., 2008). It was first launched in October 2003 onboard a DMSP F16 spacecraft, and since then, this instrument has been flown with three other DMSP satellites.

This thesis primarily focuses on the SMMR-SSM/I-SSMIS family of radiometers, as they are well-suited for generating long climate data records (CDR). However, other spaceborne radiometer systems also support snow monitoring. The NASA Aqua satellite, launched in May 2002, carried the Advanced Microwave Scanning Radiometer for EOS (AMSR-E) instrument (Kawanishi et al., 2003), which operated until October 2011. AMSR-E was succeeded by the Advanced Microwave Scanning Radiometer-2 (AMSR2) onboard the GCOM-W satellite, launched in 2012 (Imaoka et al., 2010). Additionally, China's Fengyun-3 (FY-3) satellite series, beginning with a 2012 launch, includes the Microwave Radiation Imager (MWRI) instrument (H. Yang et al., 2011). The latest satellite in this series, FY-3F, launched in 2023, carries an upgraded MWRI-II radiometer with additional channels (J. Yang et al., 2024)

2.3 Assimilation-based SWE retrieval

The assimilation approach for SWE retrieval employs a Bayesian non-linear iterative assimilation approach, first outlined in Pulliainen, 2006 and later expanded in Takala et al., 2011 and Luojus et al., 2021. The algorithm

relies on two primary data inputs: vertical passive microwave T_b measurements at around 19 GHz and 37 GHz, and daily synoptic snow depth (SD) measurements. Retrieval also utilized a snow model discussed in the next section.

2.3.1 Snow model

The HUT (Helsinki University of Technology) snow emission model is a semi-empirical, radiative transfer-based model that calculates the emission of a single-layer snowpack as a function of snow depth, snow density, and effective snow grain size (Pulliainen et al., 1999). The model also considers ground emission, forest canopy, and atmospheric effects on space-borne T_b measurements (Pulliainen et al., 1999). As the model is relatively simple (compared to theoretical models), iterative inverse solving of the model is possible.

The emitted T_b of snow at snow-air boundary is given by Pulliainen et al., 1999:

$$T_{b,snow}(\theta) = T_b(0^+,\theta)e^{-(\kappa_e - q\kappa_s)dsec(\theta)} + \frac{\kappa_a T_s}{\kappa_e - q\kappa_s}(1 - e^{-(\kappa_e - q\kappa_s)dsec(\theta)}), \quad (2.4)$$

where θ is the propagation angle of radiation (rad), $T_b(0^+,\theta)$ is the radiation from the soil (K), κ_e is the extinction coefficient ($\kappa_e = \kappa_a + \kappa_s$), κ_s is the scattering coefficient, κ_a is the absorption coefficient, and T_s is the physical temperature of snow (K). The q parameter has been determined for snow in Pulliainen et al., 1999 by fitting the HUT snow model to experimental snow slab emission data, and a good value for q was found to be 0.96 for the frequency range from 11 GHz to 94 GHz. The first term in 2.4 describes radiation from below the snow layer, and the second term describes the emission from the snow layer. The extinction coefficient κ_e is determined using an empirical equation for frequencies between 1 GHz and 60 GHz (M. Hallikainen et al., 1987):

$$\kappa_e = 0.0018 f^{2.8} d_{obs}^2, \quad (2.5)$$

where d_{obs} is the snow grain size and f is frequency. κ_a is calculated from the complex dielectric constant of dry snow. The real part is based on formulas given by Mätzler, 1987 and the imaginary part is based on the Polder-van Santen mixing model (M. Hallikainen et al., 1986).

2.3.2 Retrieval algorithm

Figure 2.2 shows a flowchart of the algorithm. Four primary steps of the SWE retrieval algorithm are explained below.

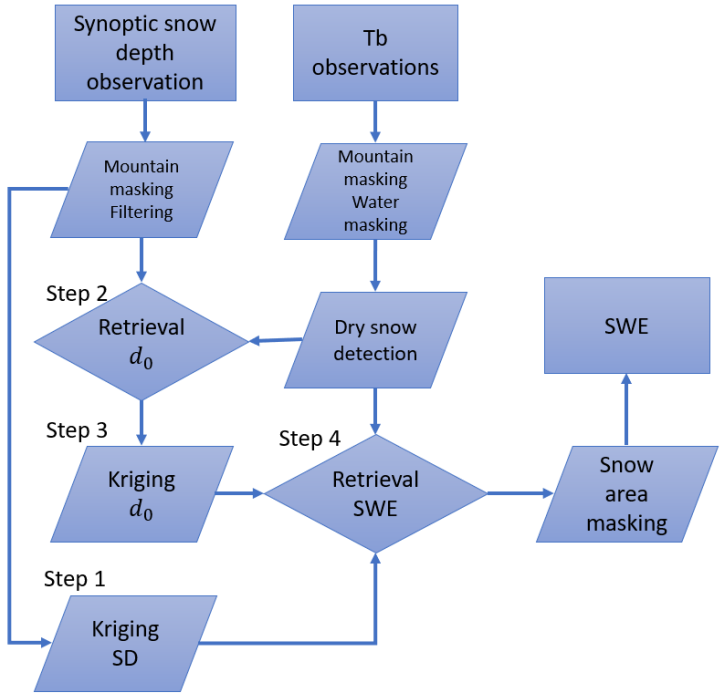

Figure 2.2. Flowchart of the assimilation-based SWE retrieval algorithm.

1. Determining background SD field: An 'observed SD' field (and its variance) are interpolated from synoptic SD observations for the day under investigation using ordinary Kriging interpolation (Oliver and Webster, 1990).

2. Retrieving Effective Snow Grain Size (d_0): Effective snow grain size values (d_0) are derived for grid cells with SD observations (actual measurements, not interpolated values) by numerically inverting the HUT snow emission model. A constant snow density of 240 $\mathrm{kg\,m^{-3}}$, deemed reasonable globally according to Sturm et al., 2010, is used. Physical temperature is assumed to be 268.15 K (or -5 °C) based on experimental data by Rautiainen et al., 2014. The model is matched to radiometer T_b observations at SD observation points by optimizing d_0. Final d_0 estimates and their standard deviations for each SD measurement location are obtained by averaging values from the six nearest SD measurements.

3. Interpolating Background d_0 field: A background d_0 field (and corresponding variances) is created by interpolating effective snow grain size estimates for pixels with SD observations, as calculated in step 2.

4. Bulk SWE Retrieval: Bulk SWE is retrieved by incorporating observed T_b ($T_{b,obs}$), derived effective snow grain sizes and their variances (from Steps

2 and 3), and the constant snow density into a numerical inversion of the HUT snow emission model. The model estimates ($T_{b,mod}$) are fitted to observations by incrementing the SD value. The background SD field from Step 1 constrains the retrieval, and the assimilation process adaptively balances T_b measurements with the background SD field, producing a final SWE estimates:

$$min_{SD}((\frac{(T^{19v}_{b,mod}(SD) - T^{37v}_{b,mod}(SD)) - (T^{19v}_{b,obs} - T^{37v}_{b,obs}))}{\sigma^2})^2 + (\frac{SD - \hat{SD}_{ref}}{\sigma_{SD,ref})^2}), \tag{2.6}$$

where $\hat{SD}_{ref}$ is the snow depth estimate and $\sigma_{SD,ref}$ is its standard deviation estimate from the Kriging interpolation. SD is the snow depth for which the equation is minimized. The variance of T_b, σ^2, is estimated by approximating ΔT_b (where $\Delta T_b = T_b^{19} - T_b^{37}$) as a function of snow depth and grain size in a Taylor series:

$$\Delta T_B(SD, d_0) \approx \Delta T_b(SD, \langle \hat{d}_{0,ref} \rangle) + \frac{\partial \Delta T_b(SD, \langle \hat{d}_{0,ref} \rangle)}{\partial d_0}(d_0 - \langle \hat{d}_{0,ref} \rangle), \tag{2.7}$$

$$\sigma^2 = var(\Delta T_b(SD, \langle \hat{d}_{0,ref} \rangle) = (\frac{\partial \Delta T_b(SD, \langle \hat{d}_{0,ref} \rangle)}{\partial d_0})^2 \sigma^2_{d_0,ref}. \tag{2.8}$$

After these four main steps are performed, snow-free areas are detected and cleared of SWE to form the final SWE estimate maps. Different methods can be used to detect snow-free areas.

2.3.3 GlobSnow v3.0 dataset

GlobSnow v3.0 (GSv3.0) dataset (Luojus et al., 2021), produced using the assimilation method, is a widely used SWE dataset. It is often used as a comparison for other SWE retrievals (e.g. J. Yang et al., 2024; Gao et al., 2023). The work in this thesis is built on the GSv3.0 dataset and this dataset is used as the baseline retrieval for which changes proposed in this thesis are compared.

GSv3.0 is produced for years 1979-2018 and it uses Nimbus-7 (1979-1987) (Knowles et al., 2000) and SSM/I-SSMIS (1988–2020) (R. Armstrong et al., 1994) Pathfinder Daily EASE-Grid 1.0 Brightness Temperature datasets. It is produced in a 25 km EASE-Grid 1.0 grid.

The synoptic SD data used is collected from multiple sources. The main sources for Eurasia are the European Centre for Medium-Range Weather

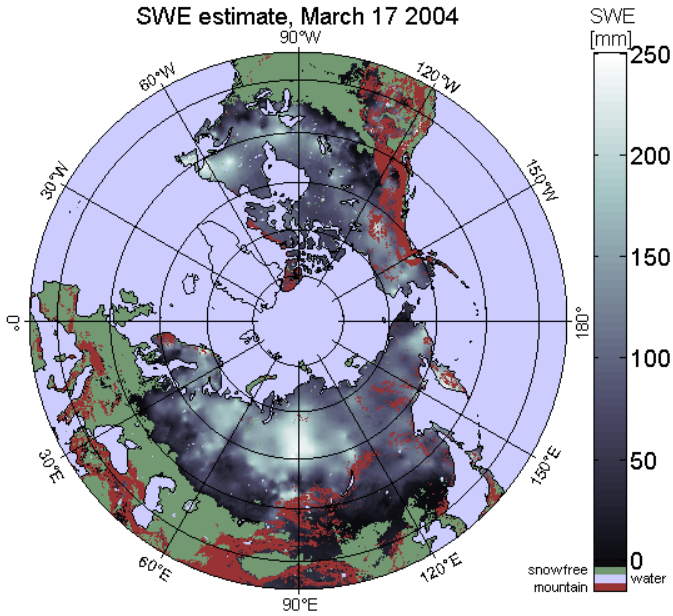

Figure 2.3. Example of GlobSnow v3.0 product for March 17 2004.

Forecasts (ECMWF) and the All-Russia Research Institute of Hydrometeorological Information - World Data Center (RIHMI-WDC) (Bulygina and Razuvaev, 2012). Global Historical Climatology Network daily (GHCNd) (Menne et al., 2012) by the National Oceanic and Atmospheric Administration (NOAA) is used as the main dataset for North America

Snow-free areas are cleared of snow in post-production using a combination of a passive microwave thresholding approach by Takala et al., 2009 and the JASMES 5 km optical Snow Extent data product (Hori et al., 2017).

3. Improving assimilation-based SWE retrieval with dynamic snow densities

Publications I and II focus on improving the assimilation-based SWE retrieval with spatially and temporally varying snow densities. Different methods were tested for developing climatological snow density fields. Fields were also applied in retrieval in two different ways: in post-production and inside the actual retrieval process.

The original assimilation-based SWE retrieval method assumes a constant snow density (240 kgm^{-3}) throughout the process. Snow density is one of the inputs required by the HUT snow model used in the SWE retrieval, and constant snow density is a known source of uncertainty in the retrieval (Takala et al., 2011). Snow density varies over time and place and is significantly influenced by the weather conditions in the location of interest. For instance, wind can break down snow crystals both on the ground and during snowfall, causing the crystals to pack more tightly and increasing the overall density (Jordan et al., 1999). Additionally, the age of the snow cover affects density as snow undergoes continuous metamorphism while on the ground (Maurice and Harold, 1981)

3.1 Climatological snow density fields

3.1.1 Creation of snow density fields

Temporal and spatial interpolation are the main steps in creating climatological snow density fields. In-situ snow density (and SWE) measurements are available from manual snow course surveys and automated stations. The frequency at which snow density measurements are made depends on the source; automatic stations produce daily data, while manual snow transect measurements are often made only every 10 or 15 days or just once a month. Thus, in many locations, there are (many) days without snow density observations, and simple linear interpolation can be utilised to estimate snow density values for the days lacking observations.

Spatial interpolation is needed to form continuous snow density maps for the northern hemisphere. In Publication I, Kriging interpolation was used for this purpose. In Publication II, Inverse Distance Weighted Regression (IDWR) interpolation was tested in addition to the Kriging interpolation. Ordinary Kriging interpolation is a geostatistical technique used to estimate values at unsampled locations by leveraging spatial autocorrelation with observed values from nearby locations (Goovaerts, 1997). Kriging interpolation was selected for Publication I as it is used successfully in other parts of the assimilation-based SWE retrieval. The IDWR modification, introduced by Emmendorfer and Dimuro, 2021, adds a new term to the standard inverse distance weighted (IDW) interpolation formula. This modification preserves the simplicity and efficiency of the traditional IDW method while reducing RMSE compared to IDW alone. When data points are limited, IDWR can achieve interpolation results comparable to, or even better than, those of Kriging interpolation. However, with a greater number of data points, Kriging generally provides superior results (Emmendorfer and Dimuro, 2021).

As only a limited amount of snow density data is available, different time aggregations of data were studied in Publications I and II. A multi-decadal approach aggregates snow density measurements from multiple decades, offering a generalized representation of snow density across this extensive period. In the multi-decadal approach, a multi-decadal average of snow densities is calculated for each day for each location with any measurements. These averages are then used to form one set of climatological density maps. The decadal version is constructed by averaging snow density data for each day of the year over a specific decade. A new set of snow density maps is needed for each decade that is studied. The annual version represents the most temporally specific approach to snow density field creation. This version was developed by constructing daily snow density maps for each individual year. Each year is treated separately, resulting in unique snow density fields that reflect the specific conditions of that year.

3.1.2 Validation of snow density fields

Overall, five different versions of snow densities were evaluated in Publications I and II. Decadal and annual snow density fields made using Kriging interpolation were included in Publications I and II. Additionally, multi-decadal Krigign interpolated fields were studied in Publication I, and IDWR interpolated decadal and annual density fields were evaluated in Publication II. As the same datasets used to create climatological snow density fields are used for validating SWE products and climatological snow density fields, these datasets were divided into implementation and validation datasets. Figure 3.1 shows locations of implementation and validation measurements in Publication II. The division of data is similar in Publication I but with less

data, as more data had become available during the writing of Publication II.

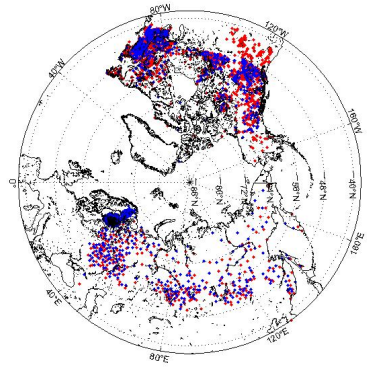

Figure 3.1. Locations of implementation (red) and validation (blue) snow density measurements. Based on Figure 1 of Publication II.

In Eurasia, annual snow density data yield the most accurate results, while in North America, decadal time aggregation provides greater accuracy. In western North America (west of 90°W), annual density data perform worse than in the eastern regions. This discrepancy may be due to the reliance on automated point data (snow pillows) in western North America, which are less representative of surrounding land cover and the broader 25 km grid cells than snow course measurements. Expanding the data pool over time, as done in the decadal product, may help offset this lack of spatial representativeness, potentially explaining the improved performance of the decadal product in western North America

Figure 3.2 compares annual, decadal, and multi-decadal Kriging interpolated snow density estimated and observed densities at validation sites. Most density values used for creating climatological snow density fields are between 150 $\mathrm{kg\,m^{-3}}$ and 350 $\mathrm{kg\,m^{-3}}$, and thus estimating values outside this range is difficult, as seen in figure 3.2. Multi-decadal and decadal versions show similar behaviour with each other, while the annual version makes somewhat better estimates of snow densities below 200 $\mathrm{kg\,m^{-3}}$ and above 300 $\mathrm{kg\,m^{-3}}$. Annual densities are made from a broader range of densities than the other two versions, which can explain the better estimation of small and large values. Multi-decadal and decadal versions are formed from averaged datasets, diminishing the effect of the highest and lowest estimates.

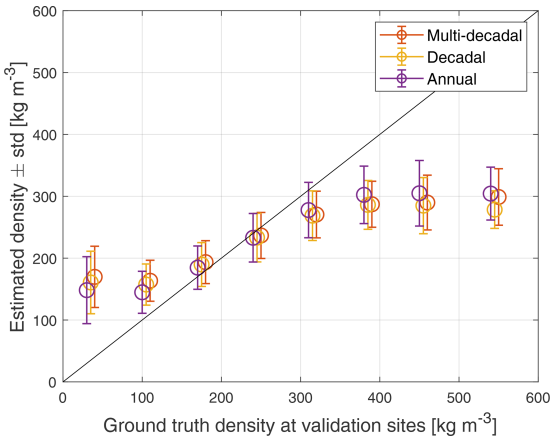

Figure 3.2. Comparison of multi-decadal, decadal, and annual density estimates. As can be observed, annual densities perform best for small and large density values. Based on Figure 6 of Publication I.

Until mid-March, the constant snow density exceeds both the IDWR and Kriging annual and decadal snow densities; after mid-March, the constant density becomes lower than the various dynamic snow densities (see Figure 3.3). Decadal densities exhibit the expected seasonal increase, aligning with the typical progression of snow densification. In contrast, annual density fields (both IDWR and Kriging interpolated) reach a peak in early April, after which snow density decreases, resulting in values lower than those commonly reported in the literature (R. Brown et al., 2019; Sturm et al., 2010). This decline may be due to snow courses being skipped in extremely wet or patchy snow conditions, which can prevent the annual datasets from fully capturing density changes during the ablation period.

The IDWR approach performs slightly better than ordinary Kriging interpolation. However, in North America, the IDWR density fields show a distinct east-west contrast not seen in the Kriging fields. This differentiation likely results from the dense network of automated snow measurements in the western United States, which more strongly influence IDWR densities than Kriging densities, as the latter employs a single variogram fitted across all of North America

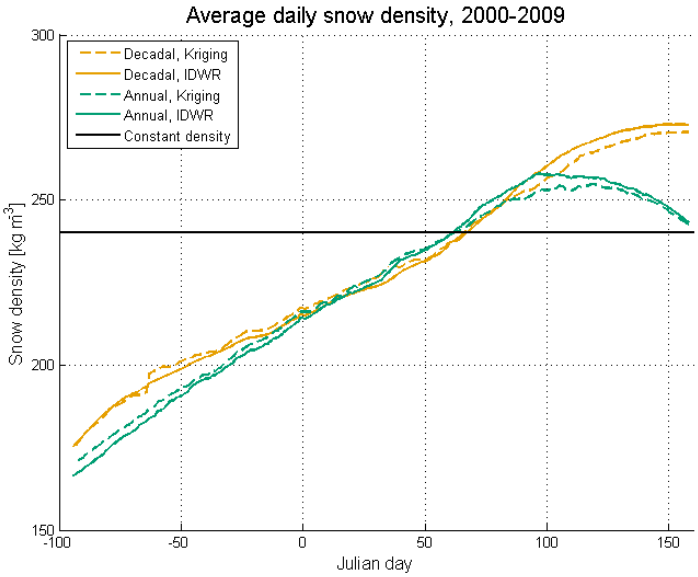

Figure 3.3. Average daily snow density between 2000–2009 for annual and decadal, and Kriging and IDWR interpolated snow density versions. The constant snow density used in the SWE retrieval procedure is also shown. Based on Figure 3 of Publication II.

3.2 Post-processing SWE retrieval with climatological snow densities

In Publication I, the climatological snow density information was used to post-process the baseline GSv3.0 SWE retrieval (Luojus et al., 2021) to study the feasibility of using these snow densities in SWE retrieval. In post-processing SWE values obtained by the retrieval are scaled with the ratio of dynamic and constant snow density:

$$SWE_{new} = SWE \frac{\rho_{dynami}}{\rho_{constant}}, \tag{3.1}$$

where $\rho_{constant}$ has value of 240 $\mathrm{kg\,m^{-3}}$. This scaling was applied to each pixel within the region where dynamic snow density data are available.

Multi-decadal, decadal, and annual versions of snow densities (made using Kriging interpolation) were first used to post-process the GSv3.0 dataset between 2000 and 2009 in Eurasia. All three versions were found to improve the baseline product, particularly by reducing the overestimation of small SWE values, as seen in Figure 3.4. Post-processing was also found to improve the underestimation of large values, but these improvements are smaller than those for small SWE values. The performance of all three post-processed versions is similar when SWE $<$ 150 mm is considered.

However, the annual version performs slightly worse than the other two versions when SWE < 500 mm is considered. The broader range of density values in annual climatological snow density maps may explain the worse performance; if the SWE estimate is close to correct, but the density used in the retrieval is far from the estimated density, post-processing causes the SWE estimate to change significantly.

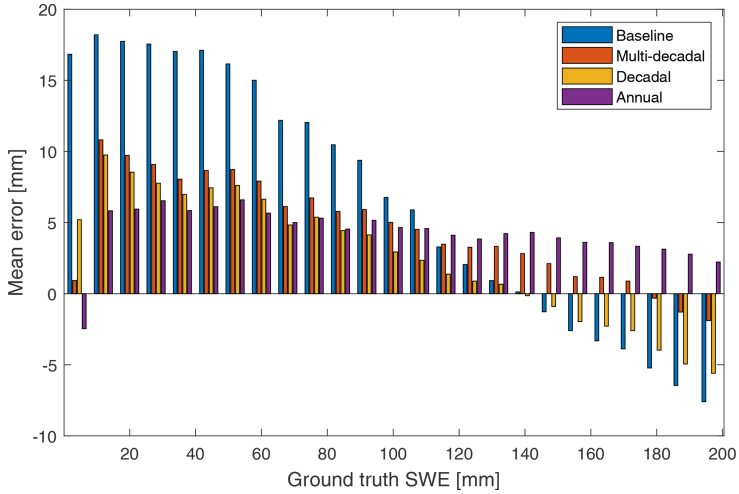

Figure 3.4. The mean error for the baseline (GSv3.0) and post-processed multi-decadal, decadal, and annual SWE estimates for Eurasia. Based on Figure 7 of Publication I.

Based on results for Eurasia from 2000–2009, the decadal snow density dataset was extended to cover all decades from 1979 to 2018 and the entire Northern Hemisphere. This expanded dataset was subsequently used to post-process the full GSv3.0 dataset. Similar to the test period, post-processing improved the accuracy of SWE estimates, particularly by reducing the overestimation of low SWE values and the underestimation of high SWE values. The constant snow density used in the SWE retrieval is generally too high in early winter and too low in late winter (as shown in Figure 3.3), and post-processing effectively addresses this issue. However, SWE underestimation for values exceeding 175 mm remains significant even after post-processing.

The most notable improvements from post-processing occur in December when the underestimation of low SWE values is most pronounced. Improvements are more substantial in Eurasia compared to North America, potentially due to differences in data collection methods. In the USA, automated point-based measurements are used, while in Eurasia, manual snow course measurements are averaged over a specific area, providing a different spatial context. Additionally, the assimilation-based SWE retrieval method performs better in Eurasia than in North America.

Post-processing alters the timing of peak snow mass, delaying it by approximately two weeks. This adjustment aligns better with the seasonal

evolution of Northern Hemisphere snow mass derived from reanalysis and model-based SWE products (see Figure 3.6). However, post-processing also reduces the total Northern Hemisphere snow mass compared to GSv3.0, which itself is biased low relative to reanalysis and model-based SWE products.

3.3 Implementing climatological snow densities into the SWE retrieval

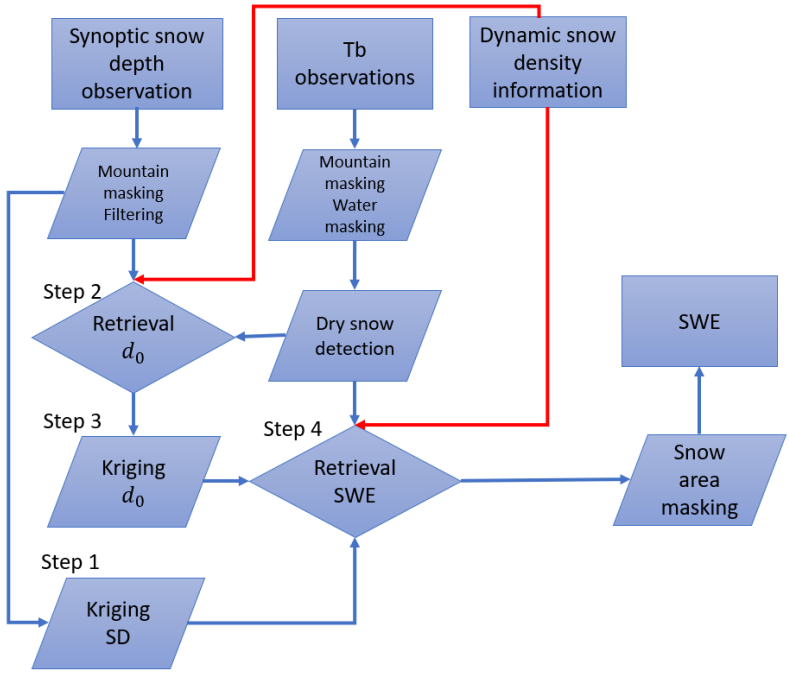

Figure 3.5. Flowchart of the assimilation-based SWE retrieval algorithm showing the addition of dynamic snow density. Based on figure 2 of Publication II.

In Publication II, annual and decadal snow densities, interpolated using IDWR and Kriging spatial interpolation methods, were incorporated into the SWE retrieval algorithm. This implementation of climatological snow densities into the assimilation-based SWE retrieval required structural modifications to the algorithm setup, as described in Section 2.3.

In Step 2, where d_0 values are determined, the HUT snow emission model was updated to use spatially and temporally varying snow density values instead of a constant density. Similarly, in Step 4, modelling was performed with these dynamic snow density values. Additionally, in Step 4, SWE was calculated from the retrieved snow depth (SD) field using the varying snow density information. These updates to the SWE retrieval process are illustrated in Figure 3.5. The impacts of dynamic snow densities on different

stages of SWE retrieval are discussed in the following sections.

Effective snow grain size
Effective snow grain size is used to account for changes in snow microstructure and is retrieved in Step 2 of the retrieval process by minimizing the error between modelled and observed Tb at locations with synoptic stations. The effect of dynamic snow densities on effective snow grain sizes is smaller than the change in snow density itself. This outcome is expected, as snow density is only one of several parameters used by the HUT emission model. Since the passive microwave brightness information remains the same for both constant and dynamic density implementations, small changes in snow density, while keeping other parameters constant, lead to minimal adjustments in grain size estimates.

Snow density influences not only the grain size estimates but also the magnitude of their variance, which affects the weight assigned to radiometer data in the final SWE estimation. When true snow density varies significantly between stations, the variance of estimated grain sizes increases. Larger variances are generally linked to less accurate grain size estimates and can reduce the influence of radiometer measurements in SWE retrieval. Dynamic snow densities can mitigate these issues by more accurately reflecting the true snow density at each location compared to a constant density. This improvement enhances effective grain size estimates and reduces their variance, ultimately contributing to more reliable SWE estimations.

SWE retrieval without final assimilation
To further study the effects of snow densities, SWE retrieval was also run without a final snow depth assimilation, meaning final SWE estimates were made by minimizing differences between modelled and measured Tb observation without constraining this process with background snow depth information. This was done for the year 2005, first using constant snow density and then using dynamic snow densities.

Dynamic snow densities improved the overestimation of SWE values in the retrieval without final assimilation. However, the dynamic snow density version had more outlier values than the constant density version, which made the RMSE and correlation coefficients worse (80.2 mm and 0.45 for the static version, and 82.3 mm and 0.39 for the dynamic version) for the dynamic density version. Most of the outlier values come from the same area in eastern Russia.

SWE retrieval
Implementing dynamic snow densities into the SWE retrieval has a bigger effect on the results than using them in post-production. Implementing snow densities into the SWE retrieval improves RMSE by approximately 4 mm, while using the dynamic snow densities in post-production improves

the RMSE by approximately 3 mm. This is expected as snow densities are used in retrieving effective snow grain size estimates and in the final numeric model inversion used for obtaining SWE estimates. However, the choice of dynamic density field (time aggregation or interpolation method) and how it is applied (in post-processing or inside the retrieval) have a smaller impact than using constant versus dynamic snow densities.

Overall, IDWR interpolated snow densities produce better results than Kriging interpolated densities. This is consistent with the IDWR densities being slightly more accurate than the Kriging interpolated densities. Additionally, using annual densities in SWE retrieval results in slightly better results than using decadal densities.

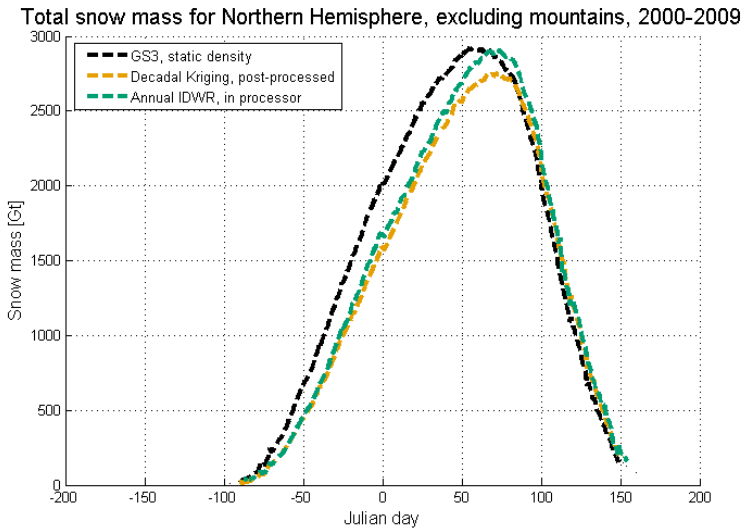

Figure 3.6. The total Northern Hemisphere snow mass (without mountains) calculated from GSv3.0 and dynamic densities in retrieval products for 2000–2009. Based on Figure 9 of Publication II.

While the differences in accuracy are not large between versions post-processed with dynamic snow densities and snow densities inside the processor, clear differences can be observed when climatological snow mass estimation is considered, as seen in Figure 3.6. Implementing varying snow densities into the SWE retrieval sifts the timing of peak snow mass in a similar manner as post-processing does. However, the reduction in peak snow mass seen in the post-processed product is much smaller or negligible when densities are implemented directly into the retrieval.

4. Improving assimilation-base SWE retrieval with bias correction

Publication III focuses on improving assimilation-based SWE retrieval with bias correction. As discussed in Chapter 2, the Tb signal saturates when the snowpack is deep and retrieving large SWE values is challenging. Assimilating SD measurements into the SWE retrieval improves the estimation of moderate snowpack, but retrieving large SWE values remains challenging.

4.1 Monthly bias correction

To improve the estimation of large SWE values and reduce the spread between different SWE products, Pulliainen et al., 2020 proposed a bias correction method. This method is based on the idea that bias is stable through time but exhibits strong autocorrelation. By pooling bias data for each grid cell over the full observational period, the method minimizes the effects of infrequent sampling while retaining interannual variability in the time series and its associated bias.

A mean SWE $BIAS_i$ (in mm) is calculated relative to the reference observations at snow course i from all observations of that particular snow course. The bias for snow course i over the whole time series is given by:

$$BIAS_i = \frac{1}{N_i} \sum_{t=1}^{N_i} (EST_{i,t} - REF_{i,t}), \tag{4.1}$$

where $EST_{i,t}$ is the radiometer estimate at the location i at time step t and similarly $REF_{i,t}$ is the snow course reference observation. After the mean bias is calculated for each grid cell with coincident snow course observations, ordinary Kriging interpolation is used to create a spatially continuous bias field. This process is repeated for each month for which bias correction is performed.

4.1.1 Updated monthly bias correction

The bias of the SWE product depends on both the reference data and the SWE retrieval itself. As new reference data have become available since the development of the bias correction method and the assimilation-based SWE retrieval algorithm has been updated, updated monthly bias fields were calculated in Publication III.

The updated reference dataset significantly improves coverage in North America, particularly with new data from Alaska, the northeastern USA, and Quebec. The amount of data available for bias correction in North America has notably increased, especially in the lowest (0–50 mm) and highest (150–350 mm) SWE bins, by more than a factor of three in the low bins, with previously minimal data in the highest bins. In Eurasia, new reference data have been added from locations in Finland, while other locations remain largely unchanged but now provide more consistent observations.

The assimilation-based SWE retrieval algorithm has also been further developed as part of the ESA Snow CCI+ project. The new bias correction was applied to the latest SnowCCI dataset, version 3.1 (SCv3.1) (Luojus et al., 2024). Key differences between SCv3.1 and the baseline GSv3.0 SWE retrieval algorithms include: 1) The satellite input dataset has been updated to a newer version, which has allowed the resolution to improve from 25 km to 12.5 km. 2) The varying snow densities studied in Publications I and II have been implemented into the operational SWE retrieval. 3) The dry snow detection algorithm and snow masks used to clear snow in post-processing have been updated.

Changes in reference data add a significant amount of snow to North America as seen in figure 4.1. The additional data increase negative bias in Quebec and Alaska while reducing the extent and magnitude of positive bias in central North America. Together, these changes add approximately 100 Gt of snow to the March snow mass. Changes in the retrieval algorithm have a smaller impact on bias and snow mass in North America compared to changes in reference data.

In Eurasia, changes in reference data have a minimal effect on the bias-corrected monthly product. However, updates to the retrieval algorithm significantly influence the bias. Specifically, the March snow mass in Eurasia decreases by approximately 100 Gt in SCv3.1 compared to GSv3.0. While the bias correction adds snow to Eurasia, SCv3.1 still has less snow than the bias-corrected GSv3.0. This reduction is largely due to the implementation of dynamic snow densities; the previously used static density was too large until March, leading to SWE overestimation.

Overall, March snow mass has stayed relatively stable in Eurasia over the 1979-2018 period. In North America, the March snow mass has a clear negative trend. This negative trend is weaker (less reduction in snow mass) for the updated SCv3.1 product than for the older GSv3.0 product.

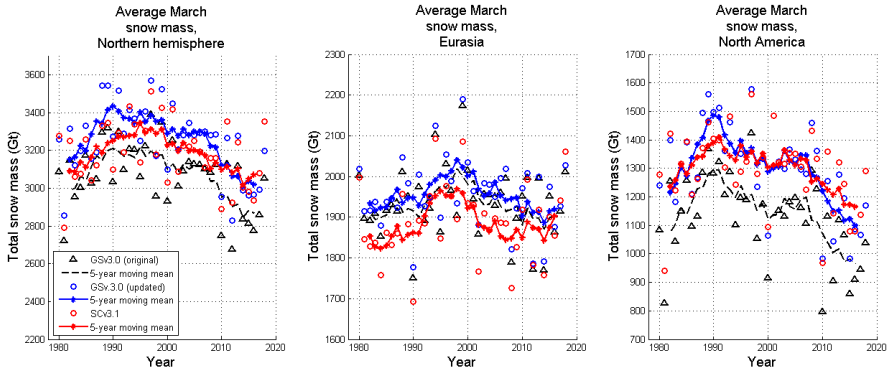

Figure 4.1. Mean March snow mass for the northern hemisphere, Eurasia and North America based on the bias-corrected GSv3.0 (black), updated bias-corrected GSv3.0 (blue) and bias-corrected SCv3.0 (red) products with the 5-year running mean (solid lines). Based on Figure 5 of Publication III.

4.2 Daily bias correction

In addition to updating monthly bias correction, bias correction was expanded to a daily time scale in Publication III. Daily bias maps were interpolated from monthly maps as a weighted means between the 15th of each month. Weights for daily bias correction are calculated as follows:

$$w_{1,i} = \frac{d_b - d_i}{d_b}, \tag{4.2}$$

$$w_{2,i} = \frac{d_i}{d_b}, \tag{4.3}$$

where $w_{1,i}$ is the weight of the bias map of the first month for i^{th} day, $w_{2,i}$ is the weight for the bias correction map of the second month for i^{th} day, d_b is the total number of days between the 15th of the first and second month and d_i is the i^{th} day from the 15th of the first month.

Daily bias maps were used to bias-correct daily SCv3.1 data through simple subtraction. Independent gamma SWE measurements from the USA and southern Canada served as validation data for the bias-corrected SWE product. This dataset was chosen for validation because the data typically used for validating SWE retrievals were already employed in the bias correction process (and thus could not be used for independent validation).

Validation using gamma SWE data shows some improvement in estimating large SWE values. However, the gamma SWE dataset provides limited spatial coverage and is not fully representative of the product's hemispheric performance. Notably, much of the higher SWE regions in the northern boreal forest are excluded. While the improvements in product accuracy are

modest (around 2 mm and 3 mm improvement in RMSE and MAE, respectively, compared to the original SCv3.1 product), the daily bias correction yields substantial enhancements in Northern Hemisphere climatological snow mass estimates.

Climatological snow mass estimation derived from SCv3.1 was compared for two ensembles of SWE products (SnowPEx1 and SnowPEx+ Mudryk et al., 2024). As shown in Figure 4.2, the uncorrected SCv3.1 product places snow mass estimates near the lower end of these ensembles. Applying daily bias correction adds approximately 500 Gt of snow mass, bringing the climatological SWE of the bias-corrected SCv3.1 product to the middle of the reanalysis product range. Additionally, Figure 4.2 demonstrates that bias-corrected SCv3.1 monthly snow mass estimates for February, April and May are notably improved compared to the monthly GSv3.0 estimates.

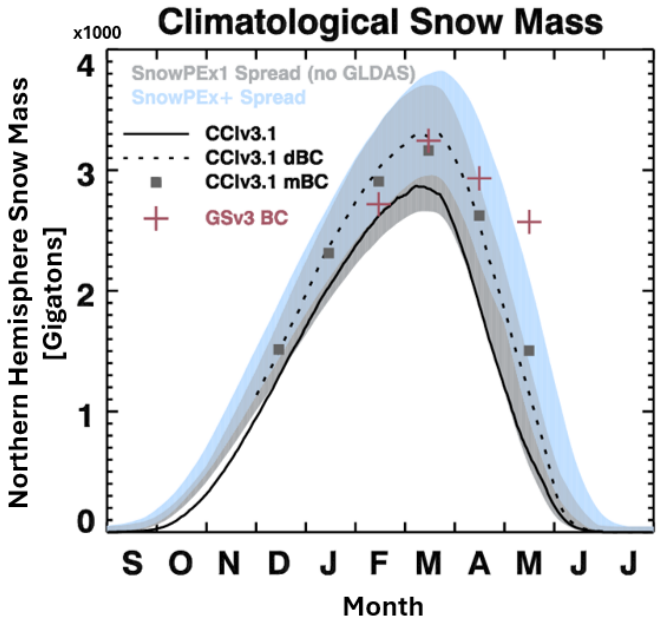

Figure 4.2. Northern hemisphere climatological snow mass 1980 – 2018, excluding complex terrain. Shading shows the range of products included in the SnowPEx (grey) and SnowPEx+ (blue) Intercomparison projects. Crosses indicate values from the GSv3.0 bias corrected monthly product, and squares show SCv3.1 bias-corrected monthly product. The dashed line shows the daily bias corrected SCv3.1, and the solid line is 'non-bias-corrected' SCv3.1 product. Based on Figure 8 of Publication III.

5. Discussion

This thesis advances PMW-based SWE retrieval methods and our ability to monitor seasonal snow cover. The accuracy of baseline SWE retrieval is improved with parametrization of snow density (Publications I and II), and the estimation of large SWE values is improved with bias correction (Publication III).

The first issue addressed in this thesis is the assumption of constant snow density in the baseline SWE retrieval. The use of a fixed snow density can lead to inaccurate SWE estimates, as it tends to overestimate SWE values early in the winter when actual snow density is lower and underestimate SWE later in the season when snow densities increase (Takala et al., 2009). In Publication I, a method was developed to create climatological snow density fields that vary both spatially and temporally. This approach was tested through post-processing of baseline SWE retrieval, which reduced the overestimation of low SWE values and the underestimation of high SWE values. Additionally, post-processing delayed the timing of peak snow mass by a few weeks, bringing it closer to modelled and reanalysis products (Mortimer et al., 2022). However, a side effect of this post-processing was a reduction in the hemispheric climatological snow mass, which was already low compared to reanalysis products in the initial retrieval.

Incorporating varying snow densities into the retrieval process can enhance SWE retrieval accuracy more than post-processing alone, as demonstrated in Publication II. The HUT snow model is employed within the retrieval algorithm to estimate effective snow grain size at weather station locations and calculate final SWE estimates via numerical model inversion. Improved snow density estimates can improve the precision of effective snow grain size estimates (and reduce their variance) and improve the modelled T_b values, which are critical for determining final SWE estimates. High grain size variance can reduce the weighting of radiometer measurements in SWE retrieval, potentially decreasing retrieval accuracy. Implementing snow densities into the retrieval improved the accuracy of the retrieval, mostly by improving the overestimation of small values and slightly improving the underestimation of large SWE values. Similar to post-processing

with dynamic snow densities, incorporating densities into retrieval delays the timing of peak snow mass and minimizes the reduction in hemispherical snow mass, achieving better results compared to using densities solely during post-processing.

Improved characterization of the seasonal evolution of snow mass is important for hydrological modelling, enabling more accurate predictions of river discharge and water availability. This is particularly critical for hydropower operations, where reliable forecasts of snowmelt runoff inform decisions on optimizing water storage and energy production (Musuuza et al., 2020). Satellite-derived snow mass estimates provide key observational data for assessing the response of seasonal snow to climate change. A comprehensive understanding of these changes is important for developing robust adaptation strategies to a warming climate.

While this thesis focuses on climatological snow densities, other methods for snow density parametrisation exist. For example, the AMSR-E SWE v1.0 product (Kelly, 2009) used temporally static but spatially varying densities from Sturm et al., 1995, while the AMSR-E v2.0 product (Tedesco and Jeyaratnam, 2016) adopted both spatially and temporally varying densities based on Sturm et al., 2010. However, when these spatially and temporally varying densities were tested in post-processing of the GSv3.0 product, they led to significant overestimations of low SWE values. Another potential approach involves using densities derived from model-based or reanalysis products. For instance, J. Yang et al., 2021, have used ERA5-land (Muñoz-Sabater et al., 2021) based snow densities as an input to the HUT model successfully. However, the utilisation of reanalysis-based snow density values would increase the correlation between remote sensing and reanalysis products themselves. Mortimer et al., 2020, suggest combining reanalysis and remote sensing products in an ensemble approach can yield improved results compared to a single remote sensing or reanalysis product, particularly when the products are as independent as possible.

Dynamic snow densities improve the accuracy of SWE retrieval more significantly in Eurasia than in North America, despite the overall reduction in snow mass originating primarily from Eurasia. In North America, notable errors occur in densely forested, high-SWE regions, particularly in the northeastern areas and mountainous western regions. Dense forests and substantial SWE values pose challenges for passive microwave SWE retrieval methods. Integrating in situ snow depth (SD) data from a sufficiently dense observation network can enhance SWE estimates in deep snow and forested regions, such as Finland (Pulliainen, 2006; Takala et al., 2011). However, in areas with sparse SD observation networks and high SD variability, like northern Quebec, SWE estimation depends more heavily on passive microwave data, which as discussed earlier, has limited sensitivity to high SWE values. Dense forest canopies further complicate retrievals, as the emission from the canopy can overwhelm the scattering signal from

the snowpack below (J. L. Foster et al., 2005; A. T. Chang et al., 1996). Although SWE is not retrieved in mountainous or complex terrain, some high mountain plateaus—often associated with high SWE—remain included, contributing to significant errors in parts of western North America.

The second key challenge this thesis examined is the limited capacity of the current PMW retrieval method to accurately measure large SWE values (SWE $>$ 150 mm). As SWE increases, the snowpack shifts from a scattering medium to a source of microwave emission, limiting retrieval skill. In Publication III, this issue was addressed with a bias correction. The bias correction method studied is based on a method introduced by Pulliainen et al., 2020. This method was updated and expanded to new months with new data in Publications III. The possibility of broadening the correction from monthly to a daily time-scale was also studied, as many applications require daily data. The daily bias correction can provide small improvements to the accuracy of SWE retrieval, and importantly, it significantly improves hemispherical snow mass estimation (around 18 % increase). Improved peak snow mass estimation is much closer to the estimation of reanalysis products, increasing the reliability of hemispheric snow mass estimation.

The addition of new snow course data influenced SWE bias correction, especially in North America. With increased data in regions like Quebec and Alaska, bias trends shifted, adding 100 Gt of snow to the hemispherical snow mass for March. In contrast, Eurasia, where data additions were minimal outside Finland, showed negligible bias changes, confirming that previous data adequately captured snow conditions in those regions. On the other hand, algorithmic updates, particularly the shift from static to dynamic snow density values, played a pivotal role in Eurasia. These changes reduced SWE overestimation caused by static density parameters, improving accuracy but lowering the uncorrected March SWE. Grid resolution differences (25 km versus 12.5 km) further influenced bias patterns, with finer resolution reducing overestimation in areas like the Kara Sea region in Siberia and mountainous terrains.

The bias fields used for correction were calculated over the entire available dataset (1979–2022). The idea behind bias correction is that bias varies spatially but is temporally stable. This allows us to combine data over a full observation period to minimize the impact of infrequent sampling. We address systematic bias but maintain the interannual variability. This holds mostly through for the new version of the SWE product and updated reference dataset, though a very small negative trend in biases is present. Given this small trend and differing accuracies among satellite platforms, it may be beneficial to perform bias correction over shorter time periods or decades. Although this reduces data volume, regions in Eurasia have maintained stable observations over the years, and new data sets obtained have significantly expanded data coverage over North America.

Simple subtraction was used for bias correction on Publication III. How-

ever, other options for bias correction are also available. For example, King et al., 2020 studied different SWE bias correction methods at local scales, finding that random forest techniques provided accurate results, suggesting a possible area for future research.

While bias correction offers a tool for improving the estimation of large SWE values, especially for long-term CDR records, the skill of PMW retrievals based on 19 GHz and 37 GHz is still limited by physics. To overcome this limitation, there have been studies of utilizing a low-frequency 10 GHz channel to improve SWE retrievals (e.g. Markus et al., 2005; Kelly, 2009). In recent years, combining active and passive microwave measurements (e.g. Zhu et al., 2021) or using solely radar data (e.g. Lievens et al., 2022; Oveisgharan et al., 2024) for SWE retrieval has also been studied. New instruments may offer good options for near-real-time evaluation, but long-term CDR product needs consistent input data, which the SMMR-SSM/I-SSMIS family of radiometers uniquely can offer.

This thesis contributes to the refinement of PMW-based SWE retrieval by addressing key limitations related to snow density and retrieval accuracy for high SWE values. These advances lay the groundwork for more reliable SWE estimates, which are important for understanding global snow mass trends and their broader environmental impacts.

6. Conclusion

This thesis focused on improving satellite-based radiometer remote sensing of SWE. The assimilation-based PMW SWE retrieval was improved through dynamic snow density parametrization and bias correction. Publication I studied the development of dynamic snow density fields, while Publication II implemented these fields into the SWE retrieval. These improvements improved the accuracy of SWE estimates, particularly for small SWE values. Additionally, the parametrization of snow density improved the seasonal evolution of SWE by delaying peak snow mass timing.

Publication III improved the bias correction approach by utilizing new in situ data and updated SWE product, and by extending the correction from a monthly to a daily timescale. These updates improved snow mass estimations for February, April, and May and improved the accuracy of large SWE estimates. The daily bias correction contributed to more reliable hemispheric snow mass assessments by significantly increasing snow mass estimates.

The outcomes of this research improve SWE product accuracy, supporting climate change monitoring, Arctic studies, and climate model validation. In particular, the improved hemispheric snow mass estimates are crucial for hydrological modelling and water resource management. Seasonal snow cover extent and duration are declining due to climate change, and SWE offers a key metric for quantifying shifts in snowfall patterns and the timing of snowmelt, both of which have broad implications for climate dynamics and hydrology.

References

Armstrong, R., Knowles, K., Brodzik, M., & Hardman, M. A. (1994). DMSP SSM/I-SSMIS Pathfinder Daily EASE-Grid Brightness Temperatures, Version 2 [Available at: https://nsidc.org/data/NSIDC-0032/versions/2 (last access: 26 May 2021)].

Armstrong, R. L., & Brun, E. (2008). *Snow and climate: Physical processes, surface energy exchange and modeling*. Cambridge University Press.

Barnett, T. P., Adam, J. C., & Lettenmaier, D. P. (2005). Potential impacts of a warming climate on water availability in snow-dominated regions. *Nature*, *438*(7066), 303–309.

Bell, V., Kay, A., Davies, H., & Jones, R. (2016). An assessment of the possible impacts of climate change on snow and peak river flows across britain. *Climatic Change*, *136*, 539–553.

Bojinski, S., Verstraete, M., Peterson, T. C., Richter, C., Simmons, A., & Zemp, M. (2014). The concept of essential climate variables in support of climate research, applications, and policy. *Bulletin of the American Meteorological Society*, *95*(9), 1431–1443.

Brown, R., Fang, B., & Mudryk, L. (2019). Update of canadian historical snow survey data and analysis of snow water equivalent trends, 1967–2016. *Atmosphere-Ocean*, *57*, 149.

Brown, R. D., & Robinson, D. A. (2011). Northern hemisphere spring snow cover variability and change over 1922–2010 including an assessment of uncertainty. *The Cryosphere*, *5*(1), 219–229.

Broxton, P. D., Dawson, N., & Zeng, X. (2016). Linking snowfall and snow accumulation to generate spatial maps of swe and snow depth. *Earth and Space Science*, *3*(6), 246–256.

Bulygina, O. N., & Razuvaev, V. N. (2012). Daily temperature and precipitation data for 518 russian meteorological stations [https://doi.org/10.3334/CDIAC/cli.100]. http://meteo.ru/english/climate/descrip9.htm

Chang, A., & Foster, J. (1987). Nimbus-7 SMMR Derived Global Snow Cover Parameters. *Annals of Glaciology*, *9*, 39–44. https://doi.org/10.3189/S0260305500200736

Chang, A. T., Foster, J. L., & Hall, D. (1996). Effects of forest on the snow parameters derived from microwave measurements during the boreas winter field campaign. *Hydrological Processes*, *10*(12), 1565–1574.

Deems, J. S., Painter, T. H., & Finnegan, D. C. (2013). Lidar measurement of snow depth: A review. *Journal of Glaciology*, *59*(215), 467–479.

Derksen, C., & Brown, R. (2012). Spring snow cover extent reductions in the 2008–2012 period exceeding climate model projections. *Geophysical Research Letters*, *39*, 1–6. https://doi.org/10.1029/2012GL053387

Dozier, J., Green, R. O., Nolin, A. W., & Painter, T. H. (2009). Interpretation of snow properties from imaging spectrometry. *Remote Sensing of Environment*, *113*, S25–S37.

Emmendorfer, L. R., & Dimuro, G. P. (2021). A point interpolation algorithm resulting from weighted linear regression. *Journal of Computational Science*, *50*, 101304. https://doi.org/10.1016/j.jocs.2021.101304

Flanner, M. G., Shell, K. M., Barlage, M., Perovich, D. K., & Tschudi, M. (2011). Radiative forcing and albedo feedback from the northern hemisphere cryosphere between 1979 and 2008. *Nature Geoscience*, *4*(3), 151–155.

Foster, J. L., Sun, C., Walker, J. P., Kelly, R., Chang, A., Dong, J., & Powell, H. (2005). Quantifying the uncertainty in passive microwave snow water equivalent observations. *Remote Sensing of environment*, *94*(2), 187–203.

Foster, J., Chang, A., & Hall, D. (1997). Comparison of snow mass estimates from a prototype passive microwave snow algorithm, a revised algorithm and a snow depth climatology. *Remote sensing of environment*, *62*(2), 132–142.

Frei, A., Tedesco, M., Lee, S., Foster, J., Hall, D. K., Kelly, R., & Robinson, D. A. (2012). A review of global satellite-derived snow products. *Advances in Space Research*, *50*(8), 1007–1029.

Gao, S., Li, Z., Zhang, P., Chen, Q., Huang, L., Zhou, J., Zhao, C., Qiao, H., & Zheng, Z. (2023). A novel global snow depth retrieval method considering snow metamorphism and forest influence. *Remote Sensing of Environment*, *295*, 113712. https://doi.org/https://doi.org/10.1016/j.rse.2023.113712

Gloersen, P., & Barath, F. (1977). A scanning multichannel microwave radiometer for Nimbus-G and Seasat-A. *IEEE Journal of Oceanic Engineering*, *OE-2*, 172–178. https://doi.org/10.1109/JOE.1977.1145331

Goodison, B. E. (1989). Determination of areal snow water equivalent on the canadian prairies using passive microwave satellite data. *12th Canadian Symposium on Remote Sensing Geoscience and Remote Sensing Symposium, 3*, 1243–1246.

Goovaerts, P. (1997). *Geostatistics for natural resources evaluation*. Oxford University Press, Cambridge University Press. https://doi.org/10.1017/S0016756898631502

Hallikainen, M., Ulaby, F., & Abdelrazik, M. (1986). Dielectric properties of snow in the 3 to 37 ghz range. *IEEE transactions on Antennas and Propagation*, *34*(11), 1329–1340.

Hallikainen, M., Ulaby, F., & Deventer, T. (1987). Extinction behavior of dry snow in the 18- to 90-GHz range. *IEEE Transactions on Geoscience and Remote Sensing*, *GE-25*(6), 737–745. https://doi.org/10.1109/TGRS.1987.289743

Hallikainen, M. T., & Jolma, P. A. (1992). Comparison of algorithms for retrieval of snow water equivalent from nimbus-7 smmr data in finland. *IEEE Transactions on Geoscience and Remote Sensing*, *30*(1), 124–131.

Hollinger, J., Piercce, J., & Poe, G. (1990). SSM/I Instrument evaluation. *IEEE Transactions on Geoscience and Remote sensing*, *28*(5), 781–790. https://doi.org/10.1109/36.58964

Hori, M., Sugiura, K., Kobayashi, K., Aoki, T., Tanikawa, T., Kuchiki, K., & Enomoto, H. (2017). A 38-year (1978–2015) northern hemisphere daily snow cover extent product derived using consistent objective criteria from satellite-borne optical sensors. *Remote Sensing of Environment*, *191*, 402–418. https://doi.org/10.1016/j.rse.2017.01.023

Imaoka, K., Kachi, M., Fujii, H., Murakami, H., Hori, M., Ono, A., Igarashi, T., Nakagawa, K., Oki, T., Honda, Y., & Shimoda, H. (2010). Global change observation mission (gcom) for monitoring carbon, water cycles, and climate change. *Proceedings of the IEEE*, *98*, 717–734.

Jordan, R., Andreas, E., & Makshtas, A. (1999). Heat budget of snow-covered sea ice at North Pole 4. *Journal of Geophysical Research: Oceans*, *104*(C4), 7785–7806. https://doi.org/10.1029/1999JC900011

Kawanishi, T., Sezai, T., Ito, Y., Imaoka, K., Takeshima, T., Ishido, Y., Shibata, A., Miura, M., Inahata, H., & Spencer, R. W. (2003). The advanced microwave scanning radiometer for the earth observing system (amsr-e), nasda's contribution to the eos for global energy and water cycle studies. *IEEE Transactions on Geoscience and Remote Sensing*, *41*(2), 184–194. https://doi.org/10.1109/TGRS.2002.808331

Kelly, R. (2009). The amsr-e snow depth algorithm: Description and initial results. *Journal of the Remote Sensing Society of Japan*, *29*(1), 307–317.

Kinar, N., & Pomeroy, J. (2015). Measurement of the physical properties of the snowpack. *Reviews of Geophysics*, *53*(2), 481–544.

King, F., Erler, A. R., Frey, S. K., & Fletcher, C. G. (2020). Application of machine learning techniques for regional bias correction of snow water equivalent estimates in ontario, canada. *Hydrology and Earth System Sciences*, *24*(10), 4887–4902.

Knowles, K., Njoku, G., Armstrong, R., & Brodzik, M. (2000). Nimbus-7 SMMR Pathfinder Daily EASE-Grid Brightness Temperatures, Version 1. https://doi.org/10.5067/36SLCSCZU7N6

Kunkee, D., Poe, G., Boucher, D., Swadley, S., Hong, Y., Wessel, J., & Uliana, E. (2008). Design and Evaluation of the First Special Sensor Microwave Imager/Sounder. *IEEE Transactions on Geoscience and Remote sensing*, *46*(4), 863–883. https://doi.org/10.1109/TGRS.2008.917980

Kunzi, K. F., Patil, S., & Rott, H. (1982). Snow-cover parameters retrieved from nimbus-7 scanning multichannel microwave radiometer (smmr) data. *IEEE Transactions on Geoscience and Remote Sensing*, (4), 452–467.

Lievens, H., Demuzere, M., Marshall, H. P., Reichle, R. H., Brucker, L., Brangers, I., & Lannoy, G. J. M. D. (2019). Snow depth variability in the northern hemisphere mountains observed from space. *Nature Communications*, *10*(1), 4629. https://doi.org/10.1038/s41467-019-12566-y

Lievens, H., Brangers, I., Marshall, H.-P., Jonas, T., Olefs, M., & De Lannoy, G. (2022). Sentinel-1 snow depth retrieval at sub-kilometer resolution over the european alps. *The Cryosphere*, *16*(1), 159–177.

Luojus, K., Pulliainen, J., Takala, M., Lemmetyinen, J., Mortimer, C., Derksen, C., Mudryk, L., Moisander, M., Hiltunen, M., Smolander, T., Ikonen, J., Cohen, J., Salminen, M., Norberg, J., Veijola, K., & Venäläinen, P. (2021). Globsnow v3.0 northern hemisphere snow water equivalent dataset. *Scientific Data*, *8*(1), 163. https://doi.org/10.1038/s41597-021-00939-2

Luojus, K., Venäläinen, P., Moisander, M., Pulliainen, J., Takala, M., Lemmetyinen, J., Derksen, C., Mortimer, C., Mudryk, L., Schwaizer, G., & Nagler, T. (2024, November 7). *Esa snow climate change initiative (snow_cci): Snow water equivalent (swe) level 3c daily global climate research data package (crdp) (1979 - 2022), version 3.1*. NERC EDS Centre for Environmental Data Analysis. https://doi.org/10.5285/9d9bfc488ec54b1297eca2c9662f9c81

Magnusson, J., Nævdal, G., Matt, F., Burkhart, J. F., & Winstral, A. (2020). Improving hydropower inflow forecasts by assimilating snow data. *Hydrology Research*, *51*(2), 226–237.

Markus, T., Powell, D. C., & Wang, J. R. (2005). Sensitivity of passive microwave snow depth retrievals to weather effects and snow evolution. *IEEE Transactions on Geoscience and Remote Sensing*, *44*(1), 68–77.

Mätzler, C. (1987). Applications of the interaction of microwaves with the natural snow cover. *Remote sensing reviews*, *2*(2), 259–387.

Maurice, G., & Harold, M. (1981). *Handbook of snow: Principles, processes, management and use*. Pergamon Press.

Menne, M., Durre, I., Vose, R., Gleason, B., & Houston, T. (2012). An overview of the global historical climatology network-daily database. *Journal of Atmospheric and Oceanic Technology*, *29*, 897–910.

Metsämäki, S., Mattila, O.-P., Pulliainen, J., Niemi, K., Luojus, K., & Böttcher, K. (2012). An optical reflectance model-based method for fractional snow cover mapping applicable to continental scale. *Remote Sensing of Environment*, *123*, 508–521. https://doi.org/https://doi.org/10.1016/j.rse.2012.04.010

Metsämäki, S., Pulliainen, J., Salminen, M., Luojus, K., Wiesmann, A., Solberg, R., Böttcher, K., Hiltunen, M., & Ripper, E. (2015). Introduction to globsnow snow extent products with considerations for accuracy assessment. *Remote Sensing of Environment*, *156*, 96–108.

Mortimer, C., Mudryk, L., Derksen, C., Brady, M., Luojus, K., Venäläinen, P., Moisander, M., Lemmetyinen, J., Takala, M., Tanis, C., et al. (2022). Benchmarking algorithm changes to the snow cci+ snow water equivalent product. *Remote Sensing of Environment*, *274*, 112988.

Mortimer, C., Mudryk, L., Derksen, C., Luojus, K., Brown, R., Kelly, R., & Tedesco, M. (2020). Evaluation of long-term northern hemisphere snow water equivalent products. *The Cryosphere*, *14*(5), 1579–1594.

Mudryk, L., Mortimer, C., Derksen, C., Elias Chereque, A., & Kushner, P. (2024). Benchmarking of swe products based on outcomes of the snowpex+ intercomparison project. *EGUsphere [preprint]*. https://doi.org/10.5194/egusphere-2023-3014

Mudryk, L., Derksen, C., Kushner, P., & Brown, R. (2015). Characterization of northern hemisphere snow water equivalent datasets, 1981–2010. *Journal of Climate*, *28*(20), 8037–8051.

Muñoz-Sabater, J., Dutra, E., Agustí-Panareda, A., Albergel, C., Arduini, G., Balsamo, G., Boussetta, S., Choulga, M., Harrigan, S., Hersbach, H., et al. (2021). Era5-land: A state-of-the-art global reanalysis dataset for land applications. *Earth system science data*, *13*(9), 4349–4383.

Musuuza, J. L., Gustafsson, D., Pimentel, R., Crochemore, L., & Pechlivanidis, I. (2020). Impact of satellite and in situ data assimilation on hydrological predictions. *Remote Sensing*, *12*(5), 811.

Oliver, M. A., & Webster, R. (1990). Kriging: A method of interpolation for geographical information systems. *International Journal of Geographical Information System*, *4*(3), 313–332.

Oveisgharan, S., Zinke, R., Hoppinen, Z., & Marshall, H. P. (2024). Snow water equivalent retrieval over idaho – part 1: Using sentinel-1 repeat-pass interferometry. *The Cryosphere*, *18*(2), 559–574. https://doi.org/10.5194/tc-18-559-2024

Planck, M. (1901). On the law of the energy distribution in the normal spectrum. *Annalen der Physik*, *4*, 1–11. https://doi.org/10.1002/andp.19013090310

Pulliainen, J. (2006). Mapping of snow water equivalent and snow depth in boreal and sub-arctic zones by assimilating space-borne microwave radiometer data and ground-based observations. *Remote Sensing of Environment*, *101*(2), 257–269. https://doi.org/10.1016/j.rse.2006.01.002

Pulliainen, J., Grandell, J., & Hallikainen, M. (1999). HUT snow emission model and its applicability to snow water equivalent retrieval. *IEEE Transactions on Geoscience and Remote Sensing*, *37*(3), 1378–1390. https://doi.org/10.1109/36.763302

Pulliainen, J., Luojus, K., Derksen, C., Mudryk, L., Lemmetyinen, J., Salminen, M., Ikonen, J., Takala, M., Cohen, J., Smolander, T., & Norberg, J. (2020). Patterns and trends of Northern Hemisphere snow mass from 1980 to 2018. *Nature*, *581*, 294–298. https://doi.org/10.1038/s41586-020-2258-0

Qu, X., & Hall, A. (2007). What controls the strength of snow-albedo feedback? *Journal of Climate*, *20*(15), 3971–3981.

Rautiainen, K., Lemmetyinen, J., Schwank, M., Kontu, A., Ménard, C. B., Mätzler, C., Drusch, M., Wiesmann, A., Ikonen, J., & Pulliainen, J. (2014). Detection of soil freezing from l-band passive microwave observations. *Remote Sensing of Environment*, *147*, 206–218.

Stöckli, R., Vermote, E., Saleous, N., Simmon, R., & Herring, D. (2005). The blue marble next generation-a true color earth dataset including seasonal dynamics from modis. *Published by the NASA Earth Observatory*.

Sturm, M., Holmgren, J., & Liston, G. E. (1995). A seasonal snow cover classification system for local to global applications. *Journal of climate*, *8*(5), 1261–1283.

Sturm, M., Taras, B., Liston, G. E., Derksen, C., Jonas, T., & Lea, J. (2010). Estimating Snow Water Equivalent Using Snow Depth Data and Climate Classes. *Journal of Hydrometeorology*, *11*(6), 1380–1394. https://doi.org/10.1175/2010JHM1202.1

Takala, M., Pulliainen, J., Metsamaki, S. J., & Koskinen, J. T. (2009). Detection of snowmelt using spaceborne microwave radiometer data in eurasia from 1979 to 2007. *IEEE Transactions on Geoscience and Remote Sensing*, *47*, 2996–3007. https://doi.org/10.1109/TGRS.2009.2018442

Takala, M., Luojus, K., Pulliainen, J., Derksen, C., Lemmetyinen, J., Kärnä, J.-P., Koskinen, J., & Bojkov, B. (2011). Estimating Northern Hemisphere snow water equivalent for climate research through assimilation of space-borne radiometer data and ground-based measurements. *Remote Sensing of Environment*, *115*, 3517–3529. https://doi.org/10.1016/j.rse.2011.08.014

Tedesco, M. (2015). *Remote sensing of the cryosphere*. John Wiley & Sons.

Tedesco, M., & Jeyaratnam, J. (2016). A new operational snow retrieval algorithm applied to historical amsr-e brightness temperatures. *Remote Sensing*, *8*(12), 1037.

Ulaby, F., Long, D., Blackwell, W., Elachi, C., Fung, A., Ruf, C., Sarabandi, K., Zebker, H., & Van Zyl, J. (2014). *Microwave radar and radiometric remote sensing*. Artech House.

Weng, Q. (2011). *An introduction to contemporary remote sensing*. McGraw-Hill Education.

Yang, H., Weng, F., Lv, L., Lu, N., Liu, G., Bai, M., Qian, Q., He, J., & Xu, H. (2011). The fengyun-3 microwave radiation imager on-orbit verification. *IEEE Transactions on Geoscience and Remote Sensing*, *49*(11), 4552–4560. https://doi.org/10.1109/TGRS.2011.2148200

Yang, J., Jiang, L., Zheng, Z., Pan, J., & Shayiran, A. (2024). A new operational northern hemisphere snow water equivalent retrieval algorithm for fy-3f/mwri-ii based on pixel-based regression coefficients. *IEEE Transactions on Geoscience and Remote Sensing*.

Yang, J., Jiang, L., Lemmetyinen, J., Pan, J., Luojus, K., & Takala, M. (2021). Improving snow depth estimation by coupling hut-optimized effective snow grain size parameters with the random forest approach. *Remote Sensing of Environment*, *264*, 112630.

Zhu, J., Tan, S., Tsang, L., Kang, D.-H., & Kim, E. (2021). Snow water equivalent retrieval using active and passive microwave observations. *Water Resources Research*, *57*(7), e2020WR027563.

Business, Economy

Art, Design, Architecture

Science, Technology

Crossover

Doctoral Theses

Aalto DT 90/2025

ISBN 978-952-64-2542-9
ISBN 978-952-64-2541-2 (pdf)

Aalto University
School of Electrical Engineering
Department of Electronics and Nanoengineering
aalto.fi